JOURNAL OF SOLID STATE CHEMISTRY **134,** 45–51 (1997)
ARTICLE NO. SC977534

Anomalous Metal–Insulator Transitions in Reduced Molybdenum Oxides, $A_4Mo_{18}O_{32}$ (A = Ca, Y, Gd–Yb) with Mo_n (n = 2, 4, 6) Cluster Chains

P. Gall,* P. Gougeon,*,[1] K. V. Ramanujachary,†,‡ W. H. McCarroll,§ and M. Greenblatt‡,[1]

*Laboratoire de Chimie du Solide et Inorganique Moléculaire, Université de Rennes 1, URA CNRS No. 1495, Ave. du Général Leclerc, 35042 Rennes Cedex, France; †Department of Chemistry and Physics, Rowan College of New Jersey, Glassboro, New Jersy 08028-1701; ‡Department of Chemistry, Rutgers, The State University of New Jersey, New Brunswick, New Jersey 08903; and §Department of Chemistry, Rider College, Lawrenceville, New Jersey 08648

Received January 6, 1997; in revised form April 29, 1997; accepted July 3, 1997

Single crystals of $A_4Mo_{18}O_{32}$ (A = Ca, Y, Gd–Yb) large enough for transport measurements were grown by high-temperature reactions or molten-salt electrolysis and their electrical and magnetic properties were investigated. The crystal structure of these phases indicates the presence of three distinctly different Mo metal atom clusters (Mo_2, Mo_4, and Mo_6), which extend in complex chains along the monoclinic b axis. The temperature-dependent resitivity displays a sharp metal–insulator transition in the range 70–120 K for the Y and all the rare earth members. The metal–insulator transition temperature (T_{IM}) was observed to increase with decreasing size of the rare earth ions. No anomalies were observed in their magnetic susceptibilities at temperatures in the vicinity of metal–insulator transition. The corresponding Ca phase, however, is semiconducting. An attempt has been made to correlate the observed physical properties with the structural arrangement of the Mo_n cluster chains. © 1997 Academic Press

Key Words: **rare earth; molybdenum; oxide; clusters; electrical; magnetic; metal–insulator transition.**

INTRODUCTION

The study of reduced molybdenum oxides with extended metal–metal bonds has attracted attention in the last two decades following the seminal discovery of $NaMo_4O_6$ (1) with *trans*-edge-shared octahedral Mo_6 cluster chains by Torardi and McCarley. Since then a number of reduced molybdenum oxides featuring a variety of cluster sizes and geometries have been identified. Some of the interesting compounds in this family are $La_2Mo_2O_7$ (2), $La_5Mo_4O_{16}$ (3), and $La_4Mo_2O_{11}$ (4) (all of which contain digonal Mo_2 clusters), $NaMo_2O_4$ (5) (containing fused rhomboidal Mo atom chains), $LaMo_{8-x}O_{14}$ (6) ($x = 0$ or 0.3) with Mo_8 clusters formed by capping two faces of an Mo_6 octahedron, and AMo_5O_8 (7) (A = alkaline earth or rare earth ion), which contain Mo_{10} clusters connected by a short bond (2.66–2.77 Å) to form infinite chains. The Mo_{10} unit can also be described as a bioctahedral cluster formed by two Mo_6 octahedral units sharing an edge. The arrangement of the cluster units in these structures is such that they extend infinitely along one or two crystallographic directions imparting low-dimensional (LD) electronic correlations. The LD electronic correlations in materials are interesting in view of their potential to exhibit physical phenomena such as charge-density-wave (CDW)-driven structural phase transitions, and in favorable cases superconductivity, at low temperatures.

We have been investigating the temperature-dependent electrical and magnetic properties of reduced molybdenum oxides with strong Mo–Mo bonds with an emphasis on the structure–property correlations. Thus, in KMo_4O_6 (isostructural with $NaMo_4O_6$ having *trans*-edge-shared Mo_6 octahedra extending along the tetragonal c axis), a broad metal–semiconductor transition was observed at $\sim$120 K and was attributed to weak Anderson-like localization of the carriers (8). The observed metallic conductivity in this system seems to be related to a short Mo–Mo contact of 2.794 Å (i.e., the distance between the apical and basal Mo atoms of the Mo_6 chain units) within the cluster chains. In contrast, a longer intercluster distance of 3.08 Å observed between the Mo_8 units in $LaMo_8O_{14}$ and $LaMo_{7.7}O_{14}$ rendered them semiconducting (9). Furthermore, the quasi LD correlations in $La_5Mo_4O_{16}$ (10) and $La_2Mo_2O_7$ (11) manifested themselves as interesting anomalies in the transport properties at 180 and 120 K, respectively; the latter is attributed to a CDW-like instability. Finally, compounds with isolated cluster units (e.g., $La_4Mo_2O_{11}$), as expected, are insulating (resistivity $>10^7$ Ω-cm) (12). However, the distinctly different structural arrangements adopted by these compounds present a formidable task in systematically correlating the physical and structural properties.

[1]To whom correspondence should be addressed.

0022-4596/97 $25.00

Recently, we investigated the electrical and magnetic properties in the isostructural family of compounds, AMo_5O_8 (A = alkaline earth or rare earth ion), that contain bioctahedral Mo_{10} clusters (13). These studies revealed an interesting evolution of physical properties depending on the nature and valence of the A cation. For example, a semiconductor-to-metal transition followed by another transition to an insulating state was observed in all compositions when the A cation was a trivalent rare earth ion. In contrast, a semiconducting behavior was observed at all temperatures when A was a divalent alkaline earth or Eu^{2+} ion. The observed variations in the transport properties have been attributed to differences in the number of electrons available for metal–metal bonding as well as the shortest distance of separation between the Mo_{10} clusters. However, the exact mechanism responsible for the metal–insulator transition remains unclear at present. To further explore the effect of the number of electrons available for metal–metal bonding on the electronic properties we have investigated in some detail the $A_4Mo_{18}O_{32}$ system (A = Gd, Tb, Dy, Ho, Er, Tm, Yb, and Y) and compared their properties with those of the isostructural analog $Ca_{5.45}Mo_{18}O_{32}$ (5). We present herein our results on the electrical and magnetic properties.

EXPERIMENTAL

Single crystals of $A_4Mo_{18}O_{32}$ have been grown by a high-temperature reaction as described in an earlier publication (14). Briefly, stoichiometric mixtures of A_2O_3, MoO_3, and Mo were sealed in a molybdenum crucible with 5% (w/w) K_2MoO_4 (to assist crystallization). The contents were then heated to $\sim$ 2200 K for 10 min and cooled to 1973 K at the rate of 600 K h^{-1} and to 1273 K at the rate of 100 K h^{-1}, followed by furnace cooling to room temperature. No evidence of the incorporation of potassium in these phases was observed by both single-crystal X-ray structure and qualitative microprobe analyses. Polycrystalline samples were prepared by heating the stoichiometric amounts of A_2O_3, MoO_3, and Mo metal in sealed silica ampoules at 1200°C for 48 h followed by furnace cooling.

Black, needle-laminate crystals of $Ca_{5.45}Mo_{18}O_{32}$ were obtained at 975°C by the reduction of a melt formed from a mixture of potassium molybdate, calcium molybdate, and molybdenum trioxide in the molar ratio K_2MoO_4: $CaMoO_4$: MoO_3 = 1.65 : 1.00 : 0.053. The reaction was carried out for 17 h using a current of 35 mA. Platinum electrodes were employed and the container was a 25-cm^3 MacDanel 997 high-density alumina crucible. The run, which was made in air, was terminated by removing the electrodes from the melt and air quenching the product. The crystals of $Ca_{5.45}Mo_{18}O_{32}$ which grew as a thick matte on the cathode plate were washed with a warm solution of potassium carbonate containing ethylenediaminetetraacetate until free of matrix.

TABLE 1
Unit Cell Parameters[a] of the $A_4Mo_{18}O_{32}$ Phases

A	a (Å)	b (Å)	c (Å)	β (deg)
Gd	9.847(5)	5.6635(7)	24.116(11)	109.74(2)
Tb	9.835(5)	5.6551(4)	24.039(13)	109.85(2)
Dy	9.825(4)	5.6509(5)	24.003(10)	109.87(2)
Ho	9.813(4)	5.6494(3)	23.940(11)	109.86(2)
Er	9.805(2)	5.6471(1)	23.907(5)	109.85(1)
Tm	9.797(3)	5.6460(2)	23.861(7)	109.91(1)
Yb	9.789(3)	5.6423(11)	23.823(5)	109.85(2)
Ca[b]	9.865(7)	5.695(7)	24.211(7)	109.82(4)
Ca[c]	9.838(4)	2.845(2)	24.184(12)	109.76(5)
Y[b]	9.817(4)	5.6496(3)	23.958(9)	109.90(5)

[a]Monoclinic, space group $p2/c$.
[b]Represents a doubled b unit cell parameter.
[c]Sample prepared by molten-salt electrolysis. Data refined in $c2/m$ space group with no doubling along the b axis.

Powder X-ray diffraction (PXD) patterns were recorded with a Scintag PAD V X-ray diffractometer or a Rigaku DMax-2 system, both of which use Cu$K\alpha$ radiation. Silicon powder was used as an internal standard. The unit cell parameters of all the phases prepared here are summarized in Table 1. Electrical resistivity measurements on selected crystals were made by a standard four-probe technique in the temperature range 4–300 K. The orientation of the crystal axes was based on crystal habit whose relationship to the crystallographic unit cell had been determined earlier by Weissenberg and oscillation photography. The I–V profiles were checked randomly at different temperatures to verify the ohmic nature of the contacts. The crystal dimensions were too small to allow four-probe measurements along any direction, other than the b axis of the crystals. The magnetic susceptibility data were recorded with a Quantum Design SQUID magnetometer in the temperature range 5–300 K using an applied magnetic field of 0.5 T on a collection of randomly oriented single crystals.

RESULTS

Only a brief description of the crystal structure is presented here as the details can be found elsewhere (5, 14, 16). The crystal structures of $A_4Mo_{18}O_{32}$ (A = Gd, Tb, Dy, Ho, Er, Tm, Yb, Y, and Ca) contain three different types of chains with repeat units—(i) Mo_4O_6 (Mo_6 octahedral cluster), (ii) MoO_3 (digonal Mo_2 cluster) and (iii) $Mo_2O_{3.5}$ (rhomboidal Mo_4 cluster)—all of which extend along the monoclinic b axis (see Fig. 1a). Interestingly, the individual chains that make up this structure are observed in a variety of other compounds. For example, the *trans*-edge-shared Mo_6 octahedral chains (Fig. 1b) seen in this structure are

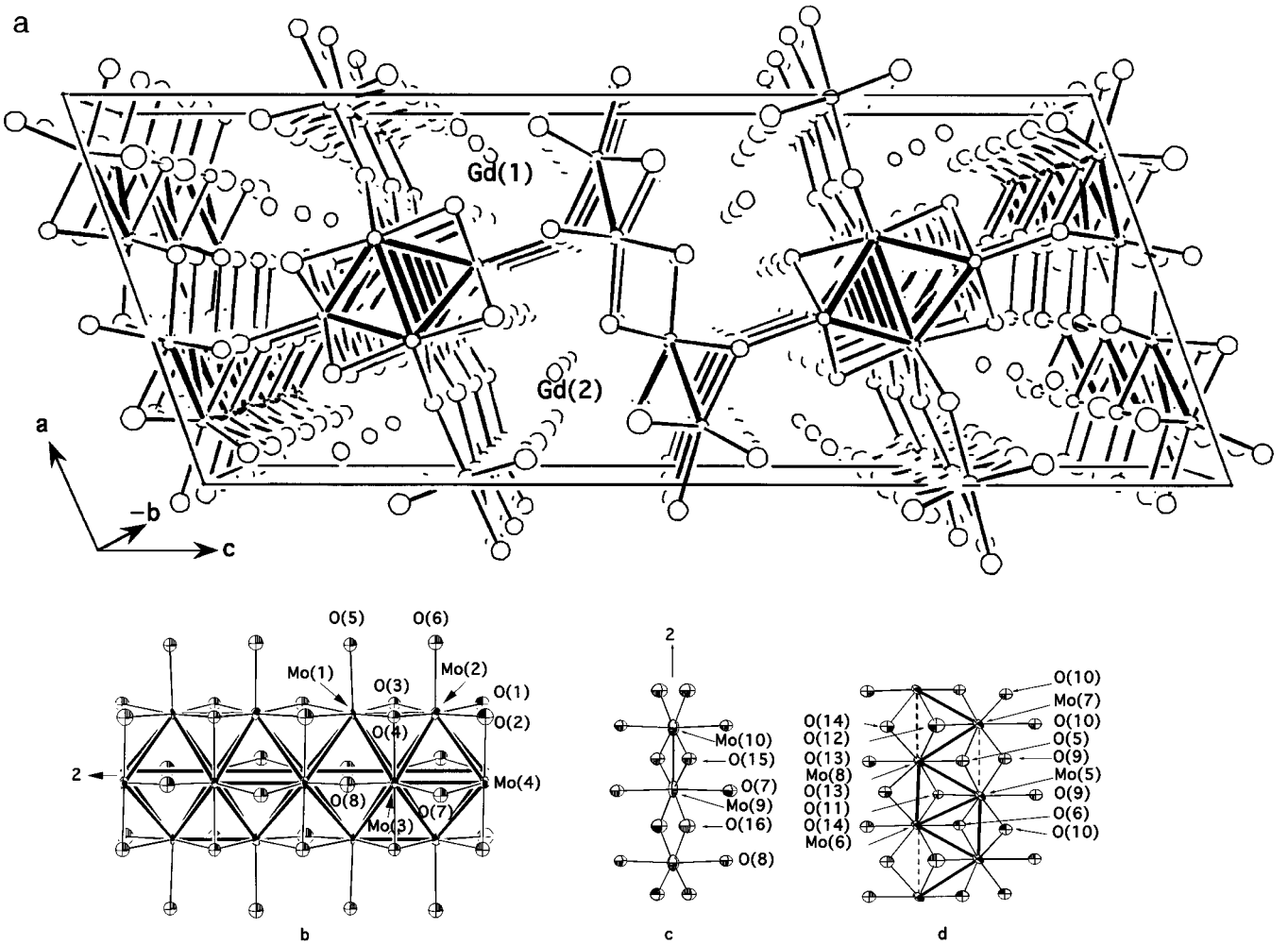

FIG. 1. (a) View of the $A_4Mo_{18}O_{32}$ structure along the monoclinic *b* axis. Formation of (b) octahedral, (c) dimeric, and (d) rhomboidal clusters that make up the individual chains in the unit cell.

similar to those found in $NaMo_4O_6$ (1), while the digonal Mo_2 chains (Fig. 1c) resemble the arrangement of Mo atoms in the distorted rutile form of MoO_2. Likewise, the rhomboidal Mo_4 chains (Fig. 1d) are similar to those found in $NaMo_2O_4$ (5). In the $A_4Mo_{18}O_{32}$ structure, the Mo_6 and Mo_2 chains are linked through oxide ions forming layers in the *ab* plane. These layers are connected to the edge-shared rhomboidal Mo_4 network in the adjacent layer. The rare earth or calcium ions are located between these layers surrounded by eight oxide ions in a bicapped trigonal prismatic coordination. However, while in $Ca_{5.45}Mo_{18}O_{32}$, the Ca^{2+} ions are delocalized over about 68% of these sites; in $Gd_4Mo_{18}O_{32}$, the Gd^{3+} ions occupy one half of them in an ordered fashion. This cationic ordering induces a doubling of the *b* unit cell parameter.

The variable-temperature electrical resistivities of all the $A_4Mo_{18}O_{32}$ single crystals measured along the monoclinic *b* axis are presented in Fig. 2. The room-temperature resistivities (ρ_{RT}) are $\sim 10^{-3}$ Ω-cm, and at temperatures above 120 K, the resistivity in all cases, increases with increasing temperature indicating metallic behavior. A transition to an insulating state is observed at a critical temperature (T_{IM}) in all the phases below 120 K. The resistivities at ~ 4.2 K were $\sim 10^3$–10^5 Ω-cm, indicating a six- to seven-orders-of-magnitude increase in the resistivity below the transition. Resistivity jumps of such large magnitudes have not been observed previously in reduced molybdenum oxides with strong Mo–Mo bonds, although similar transitions are seen at ~ 180 K in the family of so-called blue bronzes, $A_{0.3}MoO_3$ (A = K, Rb, and Tl) (15), which do not contain metal–metal bonds.

The room-temperature resistivities and the metal–insulator transition temperatures (T_{IM}) of $A_4Mo_{18}O_{32}$ (A = rare earth ion) are presented Table 2. There are no significant

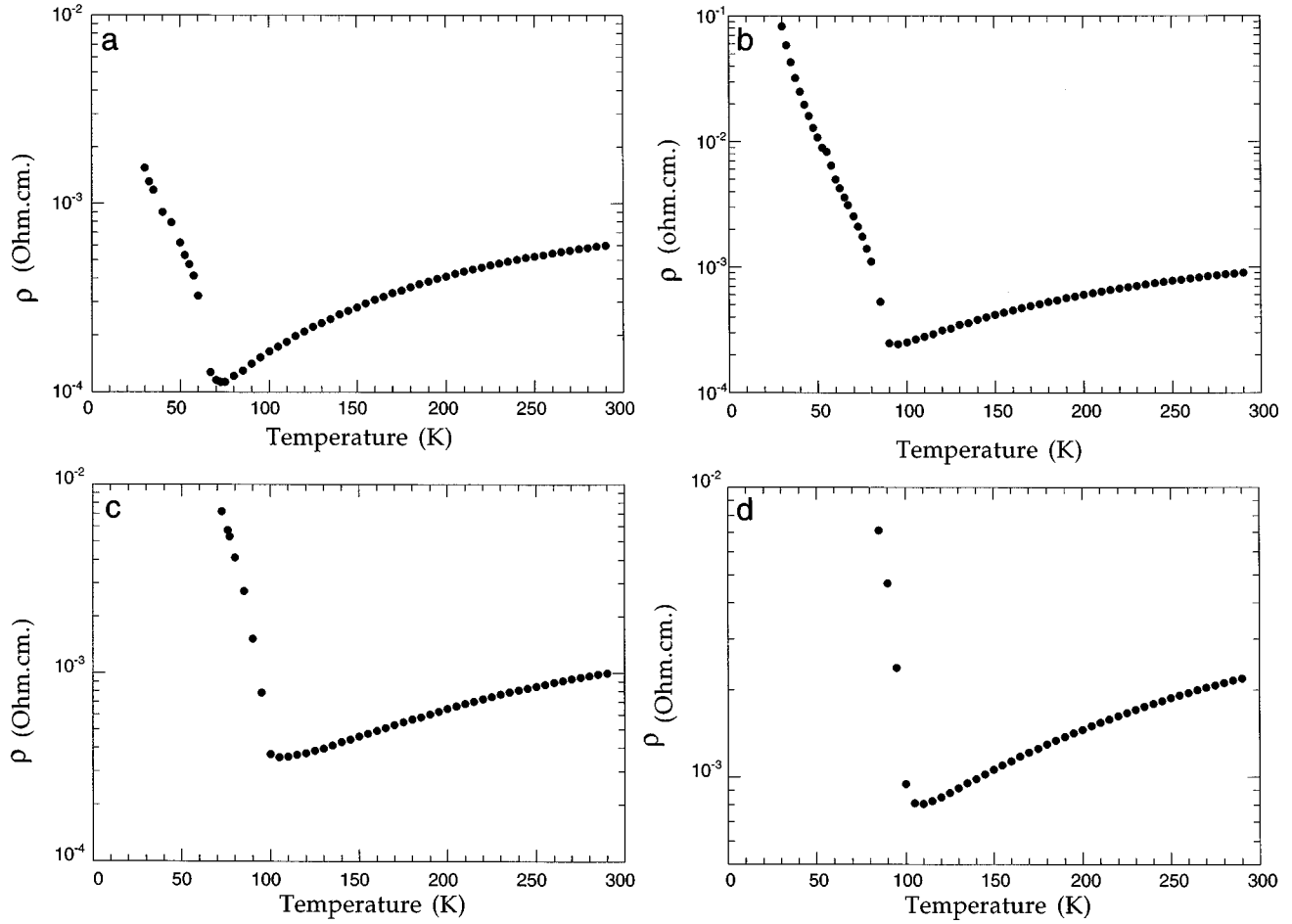

FIG. 2. Temperature variation of the electrical resistivity of $A_4Mo_{18}O_{32}$ crystals: (a) A = Gd, (b) A = Dy, (c) A = Ho, (d) A = Tm, (e) A = Yb, (f) A = Y, (g) A = Er.

differences in the ρ_{RT} of all the phases ($\rho_{RT} = 1\text{–}2 \times 10^{-3}\,\Omega$-cm); however, the T_{IM} values are sensitive to the size of the rare earth ion in $A_4Mo_{18}O_{32}$. The ρ_{RT} values indicate that the materials are poor metals, but are consistent with Mott's minimum metallic conductivity (i.e., $\rho_{RT} \leq 10^{-2}$ Ohm-cm) (17). Furthermore, such relatively high resistivities are not unusual for low-dimensional reduced molybdenum oxides (15). In Fig. 3, the linear decrease in the T_{IM} values with the increasing effective ionic radius of the rare earth ion (18) is shown. This result implies that the electronic instabilities in this system, among other factors, are strongly correlated with volume effects induced by the monotonic change of the effective ionic radii of the rare earth ion. The calcium analog, in contrast, displayed a very high ρ_{RT} of $\sim 1 \times 10^4\,\Omega$-cm, and therefore no variable-temperature measurements were attempted. In fact, the resistivity of the calcium analog at ~ 30 K was reported to be greater than 20 MΩ (16).

The temperature dependence of molar magnetic susceptibilities of selected $A_4Mo_{18}O_{32}$ crystals is shown in Fig. 4. The susceptibility data for the rare earth analogs could be fit to a modified Curie–Weiss-like behavior in the temperature range 100–300 K. Deviations observed in the Curie–Weiss relationship below 100 K could be attributed to the well-known crystal-field effects associated with the 4*f* electrons of the rare earth ions. The effective magnetic moments and the Weiss constants of all the rare earth analogs are reported in Table 2. The effective magnetic moments are in excellent agreement with the theoretically predicted values. Furthermore, the susceptibility data of the $A_4Mo_{18}O_{32}$ system (when A = magnetic rare earth ion) is clearly dominated by the paramagnetism of the 4*f* electrons, and hence the net magnetization associated with the molybdenum sublattice appears to be negligible. This is further supported by the nearly temperature-independent susceptibility of $Y_4Mo_{18}O_{32}$ ($\chi_{RT} = 5.8 \times 10^{-3}$ emu/mole), where no magnetization is expected at the rare earth site. The small upturn in the susceptibility observed below 30 K could be attributed to small amounts of paramagnetic impurities often present in

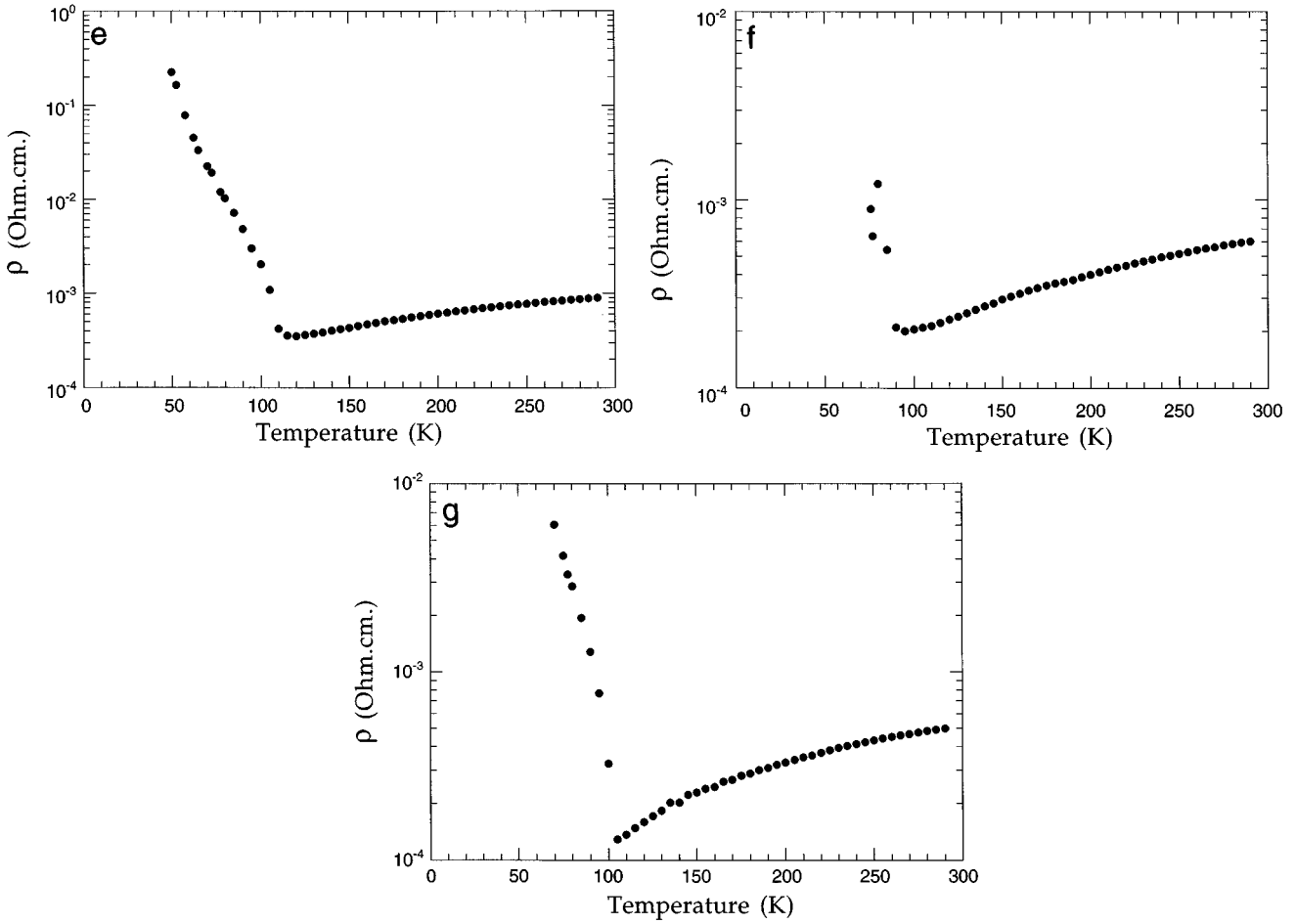

FIG. 2—*Continued*

the starting oxides used in the synthesis. However, there is no anomaly in the vicinity of the temperatures corresponding to the T_{IM} observed in the electrical resistivity.

TABLE 2
Summary of the Electrical and Magnetic Properties of the $A_4Mo_{18}O_{32}$ Phases

A	ρ_{RT} ($\times 10^{-3}$ ohm·cm)	T_{IM} (K)	μ_{eff} (Obs)[a] (B.M.)	μ_{eff} (Calc) (B.M.)
Gd	0.6	73	8.14	7.92
Tb	0.5	76	9.70	9.72
Dy	0.9	90	—	—
Ho	1.0	105	10.71	10.60
Er	0.5	105	—	—
Tm	2.2	110	—	—
Yb	0.9	120	—	—
Y	0.6	95	—	—
Ca	$\sim 10^7$	—	—	—

[a] The susceptibility measurements were performed only on selected compositions.

DISCUSSION

Although the crystal structures of $Ca_{5.45}Mo_{18}O_{32}$ and its rare earth analogs are similar to a large extent, one notes

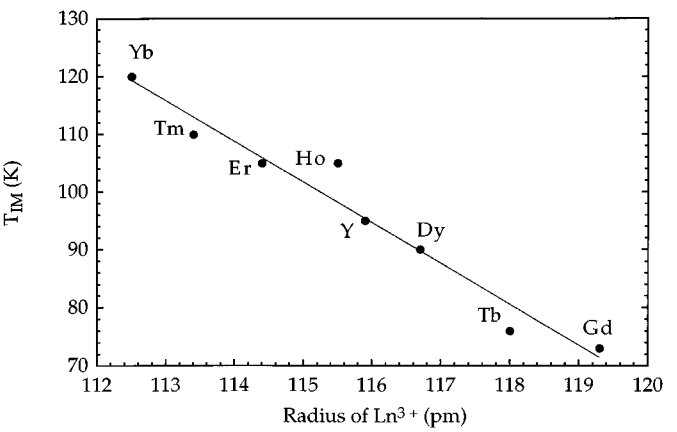

FIG. 3. Variation of T_{IM} as a function of the ionic radii of the rare earth ions in $A_4Mo_{18}O_{32}$ crystals.

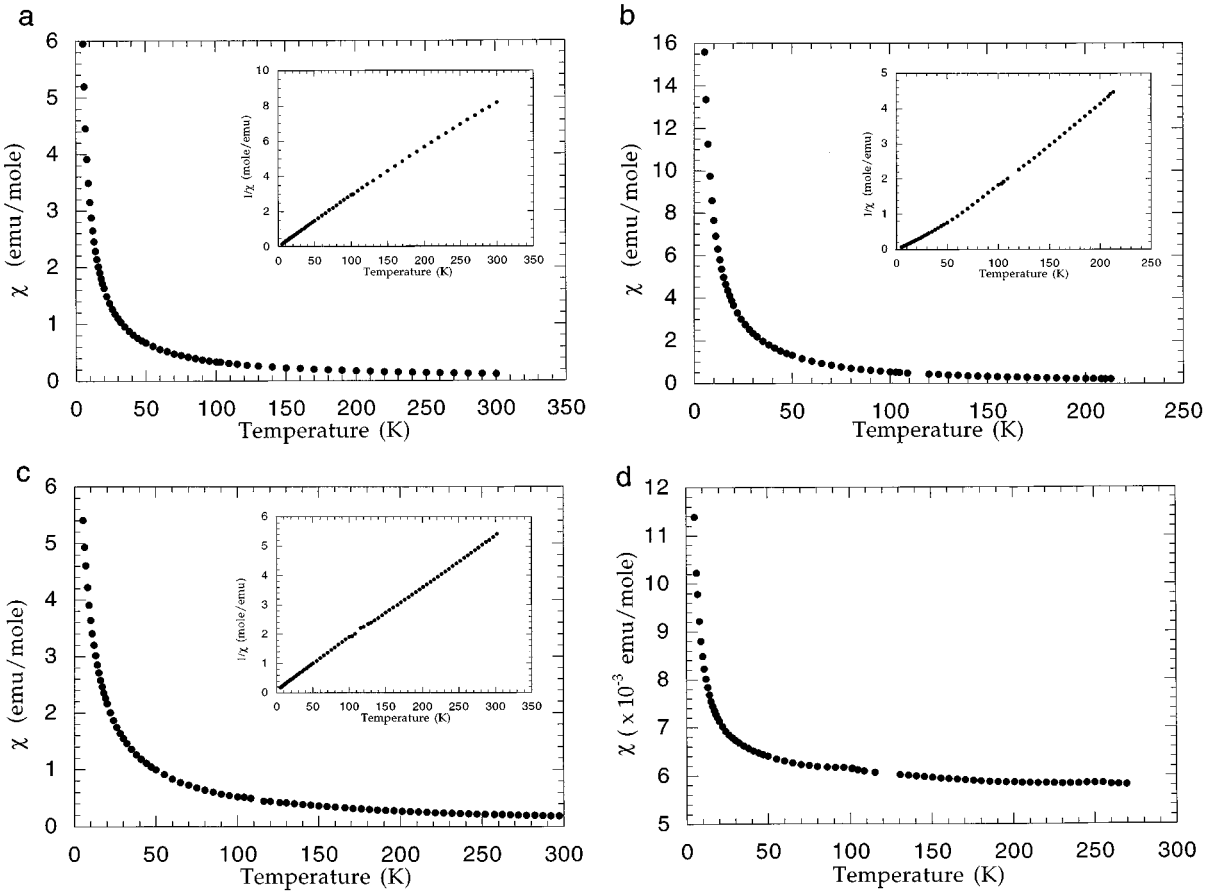

FIG. 4. Magnetic susceptibility of $A_4Mo_{18}O_{32}$ crystals as a function of temperature. (a) A = Gd, (b) A = Tb, (c) A = Ho, and (d) A = Y.

subtle differences in the intrachain Mo–Mo distances and the local geometry between these systems. These differences to a first approximation can be understood in terms of the number of electrons available for metal–metal bonding as well as the size differences in the Ca^{2+} and Ln^{3+} ions. From simple electron counting schemes, the rare earth analogs have nearly one extra electron per formula unit available for metal–metal bonding compared with the calcium analog. Nevertheless, one expects very small changes in the formal valences of the Mo atoms. For example, the average formal valence of Mo atoms in the $Ca_{5.45}Mo_{18}O_{32}$ is 2.95 compared with 2.89 calculated for the rare earth analogs. Although these differences appear to be small, they have a profound influence on the electronic transport properties. In an effort to understand the origin of these differences in the electrical conductivity of $A_4Mo_{18}O_{32}$ and $Ca_{5.45}Mo_{18}O_{32}$, we compared the Mo–Mo intracluster distances of both these compounds. The aim of such a comparison is to discern whether the extra electron in the rare earth analogs is (i) equally shared between all the cluster chains, (ii) preferentially localized in a selected chain, or (iii) distributed in a complex way. In Table 3, we list the average formal valences of Mo atoms within the three different clusters for the Ca and the rare earth analog, $Gd_4Mo_{18}O_{32}$ [calculated from bond length–bond strength correlations (19)] of Mo atoms in different cluster units. As can be seen, there are significant variations in the formal valences of Mo atoms belonging to the three different chains in both these compounds. The Mo atoms in the linear and rhomboidal cluster units, as expected, display a relatively lower oxidation state in the rare earth analog. However, the average oxidation state of Mo atoms in the octahedral cluster of $Gd_4Mo_{18}O_{32}$ (+ 2.41) is somewhat higher than in the Ca analog (+ 2.34). This suggests that the extra electron in the rare earth analogs is not equally distributed over all three different Mo_n clusters but preferentially shared by the linear single and the rhomboidal double chains. Additionally, the alternating short–long distances observed for the Mo_2 dimeric chains in both these compounds also show considerable differences. For example, in $Ca_{5.45}Mo_{18}O_{32}$ these distances are 2.560 and 3.135 Å, respectively, whereas in the Gd analog the corresponding distances are 2.572 and 3.091 Å. Thus one would expect improved correlations between the linear Mo_2 chains in the Gd analog relative to the Ca sample.

TABLE 3
Comparison of the Oxidation States of Molybdenum Atoms in Different Cluster Units of $Gd_4Mo_{18}O_{32}$ and $Ca_{5.45}Mo_{18}O_{32}$

Atom[a]		$Gd_4Mo_{18}O_{32}$	$Ca_{5.45}Mo_{18}O_{32}$
Mo1		+ 2.63	+ 2.48
Mo2		+ 2.64	—
Mo3		+ 2.21	+ 2.21
Mo4		+ 2.16	—
Average of Mo_6	octahedral chains	+ 2.41	+ 2.34
Mo5		+ 3.28	+ 3.36
Mo6		+ 3.23	+ 3.40
Mo7		+ 3.26	—
Mo8		+ 3.27	—
Average of Mo_4	rhomboidal chains	+ 3.26	+ 3.38
Mo9		+ 3.55	+ 3.76
Mo10		+ 3.56	—
Average of Mo_2	linear chains	+ 3.55	+ 3.76

[a]See Fig. 1 for the labeling scheme.

From these arguments, it is tempting to suggest that the observed metallic conductivity in all the rare earth analogs may be related to (i) increased electron density at the rhomboidal Mo clusters and (ii) enhanced correlations between the Mo_2 chains. However, in the absence of electronic band structure calculations for these structures, the foregoing discussion is merely speculative. Clearly, detailed theoretical band structure calculations are necessary to verify the proposed arguments.

The observation of a metal–insulator transition in $A_4Mo_{18}O_{32}$ (A = rare earth ion) system is also of equal interest and clearly indicates electronic instabilities at low temperatures. In an effort to understand whether this transition is due to a structural phase transition, we have carried out a detailed powder X-ray diffraction analysis of the $Gd_4Mo_{18}O_{32}$ compound at 10 K (well below the T_{IM}). Comparison of the diffraction profiles at low and ambient temperatures indicated no significant differences beyond the usual thermal expansion effects. Furthermore, we did not detect characteristic heat flow anomalies in the vicinity of T_{IM} in the variable-temperature DSC studies. These observations rule out the possibility of a first-order crystallographic phase transition being responsible for the metal–insulator transition. Furthermore, the sharpness of the transition together with the orders-of-magnitude of increase in the resistivity below the transition can not be ascribed to weak localization of carriers such as an Anderson-type transition.

Metal–insulator transitions observed in reduced transition metals with low-dimensional structures are often associated with the onset of CDW-driven phase transitions. To verify the validity of a CDW-like transition in the present system, we carried out detailed analysis of the magnetization measurements as well as current–voltage relationships at temperatures below the T_{IM}. As noted earlier, we did not see evidence of the expected decrease in the magnetic susceptibility (due to the loss of density of states near the Fermi surface), even in the $Y_4Mo_{18}O_{32}$ case, where paramagnetism due to the rare earth sublattice is absent. Furthermore, we failed to detect nonlinear transport in the I–V curves with applied threshold potentials up to 1000 mV/cm and temperatures in the range 40–120 K. A careful search for weak satellites with diffuse X-ray scattering studies is needed to confirm or rule out unambiguously the presence of the CDW state below the T_{IM} in these compounds.

ACKNOWLEDGMENTS

The support of NSF-DMR-93-14605 is acknowledged by K.V.R., W.H.M., and M.G. K.V.R. thanks Rowan College for the award of a Separately Budgeted Research Grant (No. 75958).

REFERENCES

1. C. C. Torardi and R. E. McCarley, *J. Am. Chem. Soc.* **101,** 3963 (1979).
2. A. Moini, M. A. Subramanian, A. Clearfield, F. J. DiSalvo, and W. H. McCarroll, *J. Solid State Chem.* **66,** 136 (1986).
3. M. Ledesert, Ph. Labbé, W. H. McCarroll, H. Leligny, and B. Raveau, *J. Solid State Chem.* **105,** 143 (1993).
4. P. Gall and P. Gougeon, *Acta Crystallogr. Sect. C* **48,** 1915 (1992).
5. R. E. McCarley, K. H. Lii, P. A. Edwards, and L. F. Brough, *J. Solid State Chem.* **57,** 17 (1985).
6. H. Leligny, M. Ledesert, Ph. Labbé, B. Raveau, and W. H. McCarroll, *J. Solid State Chem.* **87,** 35 (1990); H. Leligny, Ph. Labbé, M. Ledesert, B. Raveau, and W. H. McCarroll, *Acta Crystallogr., Sect. B* **49,** 444 (1993); G. Kerihuel, J. Tortelier, and P. Gougeon, *Acta Crystallogr., C* **52,** 2389 (1996).
7. S. J. Hibble, A. K. Cheetham, A. R. L. Bogle, H. R. Wakerley, and D. E. Cox, *J. Am. Chem. Soc.* **110,** 3295 (1988).
8. K. V. Ramanujachary, M. Greenblatt, E. B. Jones, and W. H. McCarroll, *J. Solid State Chem.* **102,** 69 (1993).
9. K. V. Ramanujachary, M. Greenblatt, E. B. Jones, and W. H. McCarroll, *J. Solid State Chem.* **117,** 261 (1995).
10. K. V. Ramanujachary, M. Greenblatt, W. H. McCarroll, and J. B. Goodenough, *Mater. Res. Bull.* **28,** 1257 (1993).
11. B. T. Collins, M. Greenblatt, W. H. McCarroll, and G. W. Hull, *J. Solid State Chem.* **73,** 507 (1988).
12. P. Gall, Ph.D. thesis, Universite De Rennes I, 1993.
13. P. Gall, P. Gougeon, M. Greenblatt, E. B. Jones, W. H. McCarroll, and K.V. Ramanujachary, *Croat. Chem. Acta* **68,** 849 (1995).
14. P. Gougeon, P. Gall, and R. E. McCarley, *Acta Crystallogr. Sect. C* **47,** 2026 (1991).
15. M. Greenblatt, *Chem. Rev.* **88,** 31 (1988).
16. K. H. Lii, Ph.D. thesis, Iowa State University, 1985.
17. P. P. Edwards, T. V. Ramakrishnan, and C. N. R. Rao, *J. Phys. Chem.* **99,** 5228 (1995).
18. R. D. Shannon, *Acta Crystallogr. Sect. A* **32,** 751 (1976).
19. I. D Brown, *in* "Structure and Bonding in Crystals" (M.O'Keefe and A. Navrotsky, Eds.), Vol. 2, p. 1. Academic Press, New York, 1981.